Article

Temporal Polarimetric Behavior of Oilseed Rape (*Brassica napus* L.) at C-Band for Early Season Sowing Date Monitoring

Hao Yang [1,2], Zengyuan Li [1], Erxue Chen [1,*], Chunjiang Zhao [2], Guijun Yang [2], Raffaele Casa [3], Stefano Pignatti [4] and Qi Feng [1]

[1] Institute of Forest Resource Information Techniques, Chinese Academy of Forestry, Beijing 100091, China; E-Mails: younghow@163.com (H.Y.); zengyuan.li@caf.ac.cn (Z.L.); fengqi19872005@163.com (Q.F.)

[2] Beijing Research Center for Information Technology in Agriculture, Beijing Academy of Agriculture and Forestry Sciences, Beijing 100097, China; E-Mails: zhaocj@nercita.org.cn (C.Z.); yanggj@nercita.org.cn (G.Y.)

[3] Department of Agriculture, Forests, Nature and Energy (DAFNE), Universita' della Tuscia, Viterbo 01100, Italy; E-Mail: rcasa@unitus.it

[4] Institute of Methodologies for Environmental Analysis, Consiglio Nazionale delle Ricerche, Tito Scalo (PZ) 85050, Italy; E-Mail: pignatti@lara.rm.cnr.it

* Author to whom correspondence should be addressed; E-Mail: chenerx@caf.ac.cn; Tel./Fax: +86-10-6288-9164.

Abstract: Spatial monitoring of the sowing date plays an important role in crop yield estimation at the regional scale. The feasibility of using polarimetric synthetic aperture radar (SAR) data for early season monitoring of the sowing dates of oilseed rape (*Brassica napus* L.) fields is explored in this paper. Polarimetric SAR responses of six parameters, relying on polarization decomposition methods, were investigated as a function of days after sowing (DAS) during the entire growing season, by means of five consecutive Radarsat-2 images. A near-continuous temporal evolution of these parameters was observed, based on 88 oilseed rape fields. It provided a solid basis for determining the suitable temporal window and the best polarimetric parameters for sowing date monitoring. A high sensitivity of all polarimetric parameters to the DAS at different growing stages was shown. Simple linear models could be calibrated to estimate sowing dates at early growth

stages and were validated on an independent data set. Although Volume and Span parameters provided the highest sowing date estimation accuracy at the earlier growth stages, the other four parameters (Volume/Total, Odd/Total, Entropy and Alpha) were more accurate for a wider temporal window. These results demonstrate the capability and high potential of polarimetric SAR data for monitoring the sowing date of crops in the early season.

1. Background and Rationale

The sowing date is one of the most important agronomic management practices, conditioning many aspects of crop performance along the whole growing period. Firstly, it is important for final crop productivity [1–3], which can vary by about 30% in relation to this factor [4]. In addition, it has a great influence, for example, on yield quality [5–7], water requirements and therefore irrigation management [8]. In comparison to crops sown at the optimal sowing date, fields sown excessively early are generally more vulnerable to freezing injury, while those sown too late are more susceptible to heat and drought stress [2,3], both of which cause a decrease in yield and quality. Spatial determination of the sowing date is an important input of any mechanistic or empirical crop modeling methodology [9] for regional scale yield estimation. Obtaining timely sowing date information will not only help to understand its effect on crop outputs at the regional spatial scale, but might also help to develop decision support systems for farm management, which will contribute to higher yield and better quality [2,5].

Despite the fact that the time window for optimum sowing conditions is generally not very wide, a large variability of sowing dates usually appears, even in nearby fields. This is due to subjective farmers' decisions concerning field management, such as rotations and previous crop harvesting, seeding machine limitations, or crop variety choices. In some regions of northeastern China, the sowing period for spring crops usually lasts for more than 30 days. Remote sensing data acquired by satellite sensors is extremely valuable for monitoring crop growth and phenology spatially. Various studies have been carried out using remote sensing to estimate sowing time and phenology for various crops, based on temporal profile curves of vegetation indices from optical sensors (e.g., MODIS, SPOT and NOAA/AVHRR) [10–12]. The key phenological dates, including planting date, heading date, harvesting date, and other growing periods could be determined from the curves, e.g., by detecting the maximum curvature change rates [13,14]. However, these methods, designed for regional or global scale applications, are rather coarse and inadequate for applications which have a higher demand on spatial and temporal resolution and accuracy, such as for example precision agriculture. Moreover, they require multiple images, typically capturing changing crop phenology throughout the whole growth cycle, and consequently the results can be used for sowing date estimation only at the end of the season.

As compared to optical sensors, synthetic aperture radar (SAR) sensors not only provide an increased opportunity for monitoring crops in the early season, given their acquisition capability

regardless of weather and time of the day, but can also offer additional information on crop canopy structure, e.g., from polarimetry information [15]. In recent years, the advantages provided by polarimetric SAR (PolSAR) data for agricultural monitoring have been extensively studied for applications such as crop-type classification and mapping [16,17], crop phenology monitoring [18,19], productivity assessment based on the sensitivity of polarimetric parameters to indicators of crop conditions [20], and for the retrieval of soil moisture content underneath agricultural crops [21].

Polarization target decomposition, applied to fully polarimetric SAR data, has been the most elegant and promising technique for extracting polarimetric features and physical information from the observed scattering of microwaves [22]. Previous research has indicated that polarimetric scattering decomposition may improve agricultural monitoring because of the characterization of unique scattering mechanisms from soils and vegetation biomass [23]. Specifically, two incoherent polarimetric decompositions (eigenvalue-based [24] and model-based [25] decompositions) are commonly cited and applied for agricultural applications.

Recently, experiments with satellite SAR (Synthetic Aperture Radar) data, provided by TerraSAR-X or Radarsat-2, for studying the crop phenology monitoring have been also conducted. Lopez-Sanchez, *et al.* [18,19] proved that it is possible to obtain an approximate estimation of the phenological stage of rice from stacks of X-band or C-band data. The evolution model of polarimetric observables as a function of phenology could be well established, so that the phenological stages of rice could be obtained, in most cases, without using *a priori* information. Subsequently, a more elaborate method was proposed by Vicente-Guijalba *et al.* [26] for estimating rice phenology from the combination of an evolution model with ground samples, using a Kalman filtering strategy, on the basis of a set of TerraSAR-X dual polarization images. However, their method was focused on tracking phenological development. Liu *et al.* [16] identified significant crop specific changes in scattering mechanisms as maize, wheat and soybean moved from one phenological stage to the following. Fieuzal *et al.* [27] investigated the temporal signatures of the radar backscattering intensity over rapeseed and wheat, and found that the signal dynamic depended on the crops and their associated phenological stages. Recently Wiseman *et al.* [28] were able to detect when wheat entered the milking stage, a useful indicator for the timing of harvest, when investigating RADARSAT-2 polarimetric SAR responses of 21 parameters on canola, corn, soybean, and spring wheat crops over a six-week period for a site in western Canada.

To the best of our knowledge, no previous research has explored specifically the use of SAR data to estimate the sowing dates of oilseed rape. Moreover, the microwave response of the oilseed rape crop during the growing season is much more complex with respect e.g., to rice paddies, which have a smooth underlying water surface. Previous studies revealed that the oilseed rape canopy has a strong volume scattering contribution due to its heterogeneous structure [29–31]. Specific studies aimed at the investigation of the temporal behavior of oilseed rape polarimetric response during the growing season are, however, currently unavailable.

2. Objectives

The objective of this study was, therefore, to investigate the feasibility of using SAR data for the early season monitoring of sowing dates of oilseed rape crops. To this end, multi-temporal Radarsat-2 acquisitions along an entire oilseed rape period were investigated to evaluate the potential of SAR

polarimetry at C-band to monitor the sowing date in the early season. The test site and the experimental data from SAR acquisitions of Radarsat-2 and concurrent *in situ* measurements are introduced in Sections 3 and 4. The results for sowing date monitoring at different stages are described in detail in Section 5 together with investigations on the temporal behavior of the polarimetric response of oilseed rape crops. Finally, the discussions and conclusions are presented in Sections 5 and 6 respectively.

3. Study Area

The study region is located in the Shangkuli farmland area (50°17′ to 50°23′ lat. N; 120°46′ to 120°53′ long. E), Hailar City, Inner Mongolia, China (Figure 1). The farmland, with the typical agricultural land use of Northeast China, lies on the transition zone between forest and prairie (northwest of the Greater Khingan Mountains and north of the Hulunbuir steppe). It has a cold temperate continental monsoon climate, cold and dry in the long winter, warm and wet in the short summer, supporting one harvest per year. The soil is classified as Leached Chernozem with sand clay silt texture (sand = 5.86%, clay = 42.08%, silt = 52.06%), based on three soil samples collected in the farmland. Topographic variations are minimal with slopes generally less than 1% in the farmland. Approximately 90% of the farmland is used for annual crop cultivation, principally oilseed rape and spring wheat. These crops are usually sown from May to June, reaching maturity in the middle of August, and harvested in early September. The farmland extends over 3000 hectares, with simple sowing patterns and homogeneous field parcels. A set of 88 oilseed rape fields was selected for the present study, all sown with nearly constant east-west row direction. These fields are larger than most fragmented fields in China. The area of each field ranged from 3.3 to 47.0 hectares, with a median value of 18.6 hectares.

Figure 1. Location map of the Shangkuli farmland area and oilseed rape fields; Background: Pauli-basis RGB image of Radarsat-2, acquired on 16 June 2013, as a color composite of $|S_{hh} - S_{vv}|^2$ (red), $|S_{hh} + S_{vv}|^2$ (blue), and $|S_{hv}|^2$ (green).
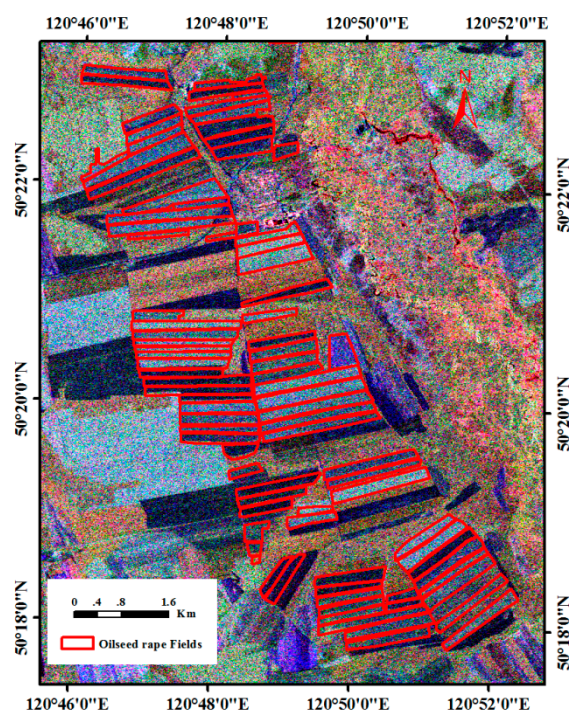
4. Approach and Methods

Five consecutive fully polarimetric C-band Radarsat-2 images were acquired in repeat pass with 24-day intervals during the growing season in 2013. All of them were acquired with the same mode, beam, and orbit pass, in order to build a time series in the most consistent way (Table 1). Their acquisition periods cover the most critical growth stages of the crop, from its sowing to its harvest, as shown in Table 2. Original Radarsat-2 images were provided in single look complex (SLC) format with pixel size of 4.73 m and 4.96 m in azimuth and ground range directions, respectively.

Table 1. Main parameters of five Radarsat-2 images.

Parameter	Values
Imaging Mode	Fine Quad Polarization
Center frequency	5.405 GHz
Incidence angle	37.4°–38.8°
Resolution	about 8m
Orbit direction	Ascending
Beam mode	FQ18
Acquired Time	UTC 09:47:33

Table 2. Acquisition dates of five Radarsat-2 images and corresponding phenological stages of oilseed rape [32].

Acquisition Dates	Principal Growth Stage [31]
23 May 2013	Germination (0)
16 June 2013	Leaf development (1) and formation of side shoots (2)
10 July 2013	Stem elongation (3), inflorescence emergence (5), and flowering (6)
03 August 2013	development of fruit (7)
27 August 2013	Ripening (8) and senescence (9)

During the seeding period in 2013, the sowing dates of all the 88 fields in the farmland were recorded. The sowing period lasted from 8 May to 31 May, with 17 different sowing dates and 24 days duration (Figure 2). Five synchronous ground measurement campaigns were carried out at each satellite overpass with a lag of no more than one day (Table 3). In each campaign,11~14 representative oilseed rape fields were surveyed for quantitative agronomic and biophysical parameters, including leaf area index (LAI), plant height, surface soil moisture, above-ground biomass (fresh and dry weight per square meter) and plant water content. LAI (m^2/m^2) was randomly measured at three sample sites within each field by LI-COR LAI-2200 instrument. Maximum LAI was observed near the beginning of flowering, but as seed development began, LAI declined with the loss of lower leaves. The top 7.5 cm volumetric water content (m^3/m^3) was also randomly measured at three sample sites within each field by FieldScout TDR 300 (Time Domain Reflectometry) Soil Moisture Meter in High Clay mode after its calibration. At each of the three sample sites, five soil moisture readings were taken resulting in 15 moisture readings per field. High soil moisture values were reached on 3 August, when a heavy rainfall had just passed. One biomass sample was collected for each field in a square of 0.5 m × 2 rows.

Each biomass sample was weighed wet, dried in a dryer at 95 °C for at least 48h and then reweighed, providing wet and dry biomass (g/m^2) as well as plant water content ((wet−dry)/wet, g/g). The dry biomass increased with the crop age. The phenological growth stage using the Biologische Bundesanstalt, Bundessortenamt and Chemical (BBCH) scale [32] was recorded.

Figure 2. The frequency distribution of oilseed rape sowing dates recorded for the 88 fields of the study area.
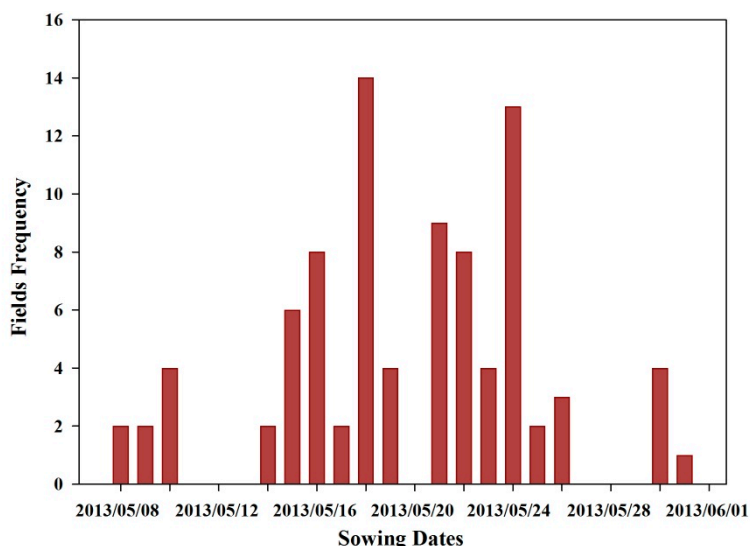

Table 3. Description of the ground measurements over oilseed rape fields. The minimum, maximum (into brackets) and mean values of these observed fields were given for each parameter.

Date	Number of Fields	DAS	LAI (m^2/m^2)	Soil Moisture (%)	Dry Biomass (g/m^2)	PWC (g/g)
23 May 2013	14	[−7, 15]	-	[19.2, 42.4] 32.7	-	-
16 June 2013	11	[16, 39]	[0, 1.5] 0.6	[32.5, 43.8] 37.8	[9.5, 89.0] 37.7	[0.88, 0.92] 0.90
10 July 2013	12	[40, 63]	[2.5, 3.6] 3.1	[34.1, 47.4] 41.7	[86.8, 350.9] 207.3	[0.86, 0.94] 0.90
03 August 2013	14	[64, 87]	[2.2, 3.5] 2.9	[41.0, 59.8] 56.3	[694.7, 2009.2] 1210.4	[0.81, 0.86] 0.84
27 August 2013	11	[89, 110]	-	[22.4, 51.0] 41.3	[875.0, 2509.7] 1616.4	[0.38, 0.75] 0.46

Note: On 23 May, the leaf area index (LAI), biomass, and PWC (plant water content) could not be measured since the fields were just being sown; On 27 August, the LAI could not be measured since no leaves were left in this period. DAS = days after sowing.

In addition, GIS data for recent years, including information about the crop type, crop varieties, the area of each field, and whether or not the land had been ploughed before seeding, was provided by the farmland administrator. An automatic meteorological station (MidWest, WPH1-PH-6) was installed in the center of the farmland for collecting agrometeorological data. Daily precipitation and mean air

temperature recorded during the 2013 growing season are shown in Figure 3. The cumulative precipitation during the seven days before each satellite acquisition date was 6.4 mm, 45.3 mm, 73.8 mm, 180.2 mm, and 4.4 mm, respectively.

Figure 3. The daily precipitation and average temperature (from 13 May to 30 August 2014); the five vertical dash lines indicate synthetic aperture radar (SAR) observation dates (23 May, 16 June, 10 July, 3 August, 27 August).
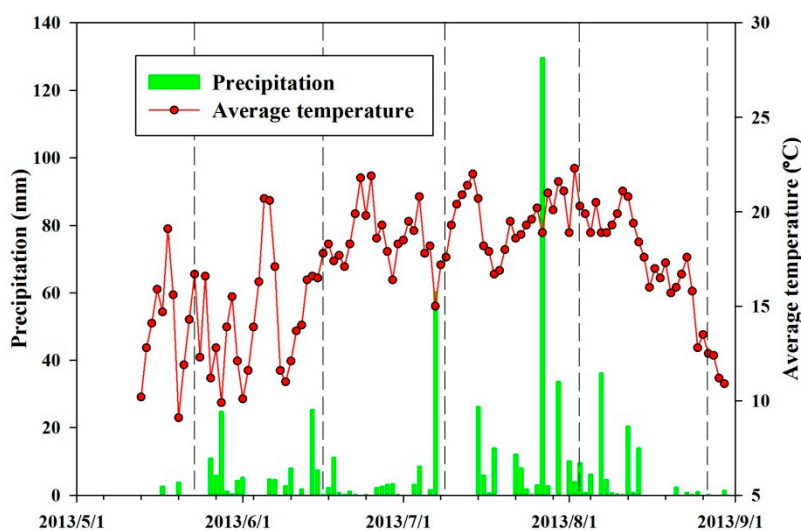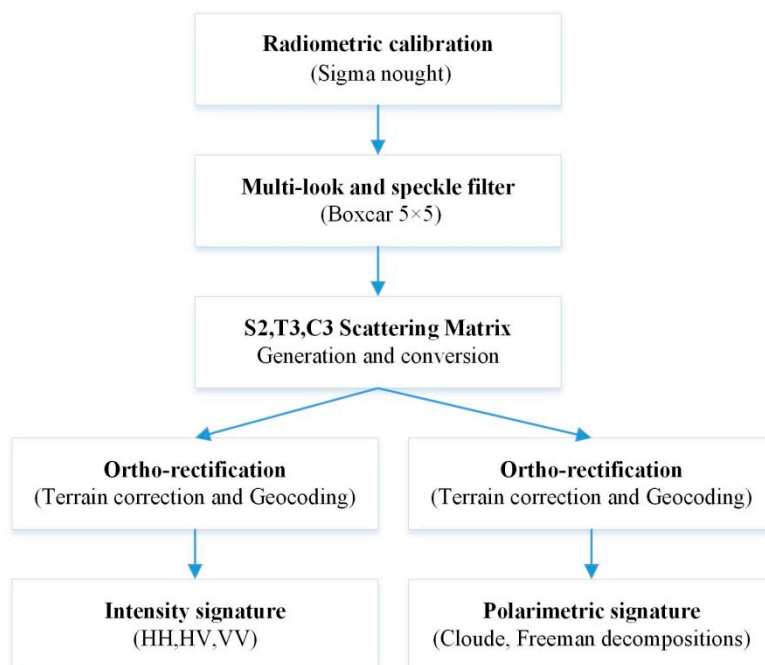

Figure 4. Flowchart of preprocessing of Radarsat-2 data.

4.1. Preprocessing of SAR Image

The quad-pol Radarsat-2 imagery was processed and analyzed as shown in the flowchart in Figure 4. Radarsat-2 quad-pol SLC data were provided as a Stokes matrix for each slant range pixel. Firstly, with the help of PolSARPro software (version 4.2, from the European Space Agency),

radiometric calibration was carried out using a look-up table in product file, to transform the digital number of each pixel (amplitude of the backscattered signal for pixel *i*, DN_i) into backscattering coefficient (σ_i^0) [33]. The data were then multi-looked and filtered using a 5 × 5 boxcar filter to suppress speckle. The filtered SAR images were then ingested to form a scattering matrix (*S2*), and then converted to a symmetrized 3 × 3 covariance matrix (*C3*) and coherent matrix (*T3*), which averages the cross-pol backscatter into a single cross-pol value [34]. Then the datasets were ortho-rectified in Mapready software (version 3.1, from the Alaska Satellite Facility), where Range-Doppler model was used for DEM-simulation and registration. The 30 m ASTER GDEM was used to simulate the SAR image according to its imaging geometry and available orbit information in the metadata, and the real SAR image was matched to the simulated image, warping to the DEM coordinate system [35,36]. After the terrain correction, the dataset was geocoded into Universal Transverse Mercator (UTM) map projection. For mathematical details of these procedures, the reader is referred to Boerner *et al.* (1998) [37].

4.2. Derivation of the Polarimetric Parameters

Polarization target decomposition techniques were used to derive a set of different parameters from the Radarsat-2 data. The Freeman-Durden three component decomposition [25] and Cloude-Pottier decomposition [24] were used in this study (Figure 4). Freeman-Durden method, as a physical scattering model-based decomposition, decomposes the backscatter response into three categories of volume scattering (noted as Volume) modeled as a set of randomly oriented dipoles, the double-bounce scattering modeled by a dihedral corner reflector, and surface or single-bounce scattering (noted as Odd) modeled by a first-order Bragg surface scatter [25]. Whereas the three scattering components indicate the absolute scattering power, their ratio to the total scattering was also used to reflect the contribution of each scattering mechanism (noted as Volume/Total, Odd/Total).

In contrast, the eigenvalue-based Cloude-Pottier decomposition does not partition the energy into these three processes, but does predict the dominant scattering type and its relevance [24]. It decomposes the coherency matrix into different eigenvectors and eigenvalues, which classify and describe the primary scattering mechanisms. The scattering entropy (noted as Entropy) and the average alpha angle (noted as Alpha) are two of the most cited parameters. Entropy, ranging from 0–1, represents the randomness of the scattering process from isotropic scattering (Entropy = 0) to totally random scattering (Entropy = 1), and is theoretically associated with depolarization effects of target features. Alpha can be used to discriminate between the three dominant scattering mechanisms. In addition, Span is the total scattering power in four polarizations and is not a parameter generated by the decomposition, but is used to represent intensity. Therefore, six polarimetric parameters (Volume, Volume/Total, Odd/Total, Entropy, Alpha, and Span) were used for the analysis carried out in the present study.

4.3. Analysis of the Temporal Evolution of Polarimetric Parameters and the Retrieval of the Sowing Dates

The temporal evolution of polarimetric response of oilseed rape crops during the entire growing season was analyzed as a function of the number of day after sowing (DAS), with the objective of

determining the optimal temporal window and the suitable polarimetric parameter for sowing date monitoring. The DAS of each field was obtained for each observation date. The polarimetric parameters were averaged at the field level. Averaging of the SAR image pixels inside a field was necessary to overcome the intrinsic speckle effect. Unlike previous analysis usually based on a small number of fields [18,19], the temporal analysis in this study was based on 88 fields. Since these fields had different sowing dates (17 sowing dates as shown in Figure 2), the status of oilseed rape fields at 17 different DAS was observed for each SAR acquisition. Therefore, overall, the status of oilseed rape fields at 85 different DAS was observed with our dataset of five consecutive SAR acquisitions. In this study, mean values of all the fields at the same DAS (the same sowing date) were calculated, for all six polarimetric parameters, in order to reduce the influence of uncontrolled factors on polarimetric parameters differences for the same DAS. The number of oilseed rape fields with the same sowing date varied from 2 to 14 (Figure 2).

Then the sensitivity of the six polarimetric parameters to the DAS was analyzed quantitatively at different growing stages. The sowing date estimation model was proposed for different polarimetric parameters. A subset of 75% of our data (66 fields) was randomly selected and used to calibrate the models for the sowing date estimation of each oilseed rape field. The remaining 25% of our dataset (22 fields) was used for validation. The performance was quantified by root mean square error (RMSE).

$$RMSE = \sqrt{\frac{1}{n-1}\sum_{i=1}^{n}(y_i - \hat{y}_i)^2} \tag{1}$$

where y_i and $\hat{y}_i$ are measured values and predicted values, and *n* is the number of observations.

5. Results and Discussion

5.1. Temporal Behavior of the Polarimetric Response during the Crop Growing Season

The temporal evolution of different polarimetric features of oilseed rape fields during the whole growing season as a function of DAS is illustrated in Figure 5. The results demonstrated SAR polarimetric response behavior at different phenological stages. The growing cycle was divided into five stages corresponding to the image acquisition dates: Stage A (BBCH stage 0), Stage B (BBCH stage 1, 2), Stage C (BBCH stage 3, 5, 6), Stage D (BBCH stage 7), and Stage E (BBCH stage 8, 9) [32]. It should be mentioned that some fields had not yet been sown on 23 May (first SAR acquisition date), and some fields had been already harvested on 27 August (last SAR acquisition), hence these fields were excluded from Figure 5.

As shown in Figure 5a,b, similar trends were observed in the evolution of the Span and Volume parameters. At the first acquisition date, most oilseed rape fields had just been sown or were at the beginning of crop emergence. The oilseed rape leaves were just emerging through the soil surface with plant heights not exceeding 5 cm. At such an early stage, the vegetation was so small that it was not visible to Radar, and hence the soil component dominated the SAR response, in accordance with previous studies [19,38]. SAR backscattering was thus mainly influenced by soil roughness and moisture (which ranged from 19.2% to 42.4%, Table 3). Indeed, as shown in Figure 6 (DAS from 1 to 15), tillage

practices, crop residues and weeds were contributing to the fluctuation of scattering of different fields. These explain the relatively low values and the variations of Span and Volume at the Stage A in Figure 5.

Figure 5. Temporal evolution of six polarimetric parameters based on 88 fields over five acquisition dates (23 May, 16 June and 10 July, 3 August and 27 August): (**a**) Span; (**b**) Volume; (**c**) Volume/Total; (**d**) Odd/Total; (**e**) Entropy; (**f**) Alpha. Each data point is the average value of all the fields having the same sowing date. The fields not sown on 23 May (DAS < 0) and harvested on 27 August are not shown.
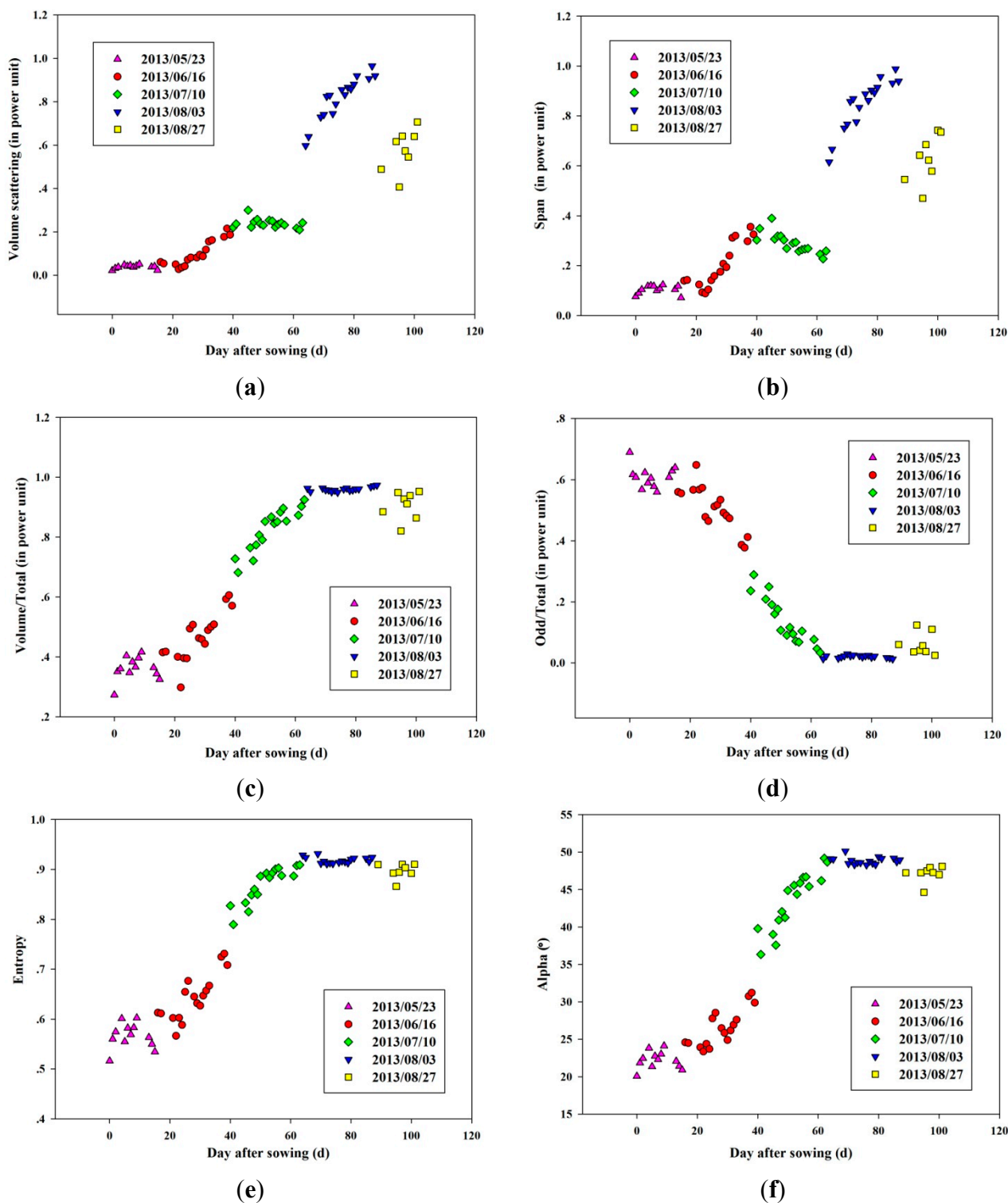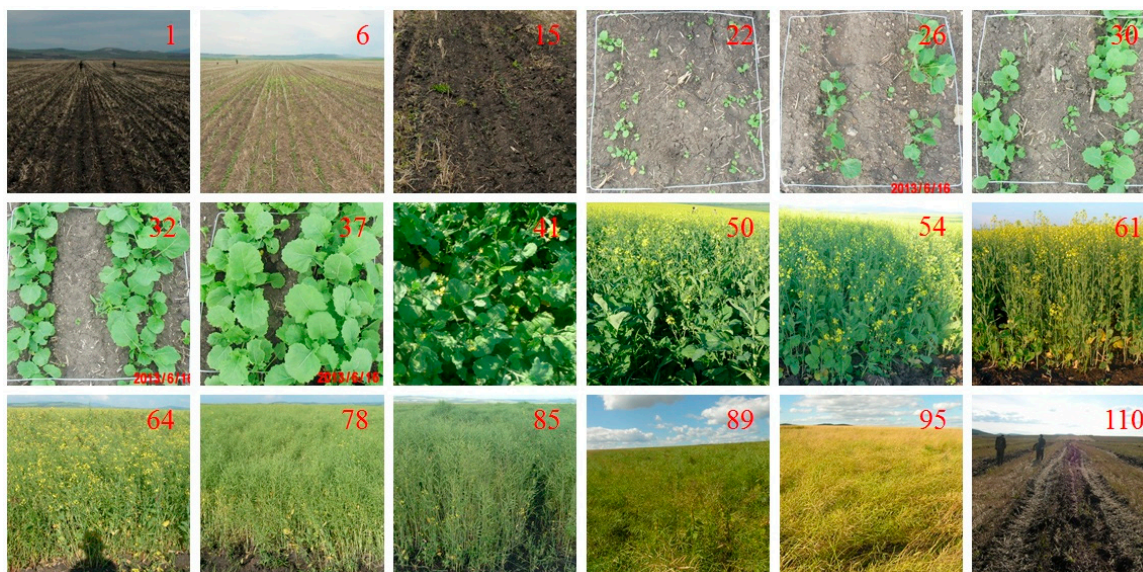
Figure 6. Typical oilseed rape fields at different days after sowing (DAS). The number in the upper-right corner of every image is its DAS value.

At Stage B, both scattering parameters increased rapidly. At this stage, oilseed rape leaves developed and became larger (6.6 cm average leaf width). The size of the leaves was comparable to C-Band wavelength (5.6 cm) and thus greater vegetation scattering results with increase of Span and Volume. As the crop developed to Stage C, a significant decline in Span was observed in Figure 5a, which was not reported by other studies [29,31,38], which were probably limited by their observation frequency. At this stage, large leaves in the bottom canopy layer began to wither and fall and resulted in smaller and less leaves in a unit volume, typically stem elongation occurred at the same time. It was in line with the LAI measurement of a typical observed field which decreased from 3.6 (DAS = 41) to 2.5 (DAS = 63) during this stage (Table 3). As a result, less microwave power was intercepted and scattered by the canopy, which explained the decrease of Span and Volume parameters. At Stage D, the oilseed rape began to pod. With the increase of pod size and number, a thick volume of pods created significant multiple scattering and increased the Span and Volume values. When the crop entered into Stage E, the oilseed rape began to ripen with decline of plant water content (from 0.84 to 0.46, Table 3), thus more wave penetration into the soil resulted in a decrease of Span and Volume. More interestingly in Figure 5a,b, there was a bounce phenomenon between Stage D and Stage E. Presumably, it was assumed that the bounce was largely attributed to rainfall events at the end of July and beginning of August, which made the backscatter signal increase sharply. Such a conjecture was supported by Figure 3, which showed persistent heavy rain exceeding 180.2 mm during the seven days before the satellite acquisition on 3 August. The increase of the backscattering signal can be due to the increase of soil moisture (from 41.7% to 56.3%, Table 3) and water standing on the plant canopy after rainfall. The rain effect on backscattering of plant canopies had also been observed in previous studies [18,39,40].

On the contrary, the temporal evolution of the other four polarimetric parameters showed a much more regular continuous trend during the whole growing season (Figure 5c–f). There was no distinct bounce phenomenon between the two last acquisition dates, with respect to Figure 5a,b. In Figure 5c, following a relatively low level at Stage A, the volume scattering ratio in total scattering (Volume/Total) kept increasing in both Stage B and Stage C. However, the increase stopped and a

saturation effect arose at Stage D. At this stage, volume scattering accounted for almost the total scattering, reaching up to 96%. This was consistent with previous reports [29–31,41], which indicated that oilseed rape was dominated by volume scattering due to its heterogeneous canopy. Then at the ripening stage (Stage E), the Volume/Total decreased slightly due to the vegetation drying. The parameter Odd/Total had totally opposite temporal behavior with respect to Volume/Total (Figure 5d). The highest value of Odd/Total appeared at Stage A, then it decreased dramatically at both Stage B and Stage C. It reached the bottom at Stage D, when the Odd scattering almost disappeared. As the oilseed rape crop becomes ripe, the Odd/Total increased due to the radar penetration capability. The parameters Entropy and Alpha had similar behavior to Volume/Total during the whole growing season (Figure 5e,f). They also suffered a saturation effect at Stage D. The increase of Entropy reflected a greater randomness of scattering. This can be attributed to a nearly random volume structure of the canopy resulting in a high entropy. Moreover, the observed seasonal trend of Alpha was in accordance with McNairn's results [41], which showed that Alpha increased during the growing season accompanied by the transition between odd scattering and volume scattering (less than or greater than 45°, respectively).

Therefore, it can be expected that the last four parameters (Volume/Total, Odd/Total, Entropy and Alpha) were independent of absolute level variations with respect to Span and Volume parameters. They seemed less sensitive to changes in environmental conditions, such as rainfall. More importantly, it was found that the four parameters increased linearly and consecutively with the DAS during the vegetative stages (from BBCH stage 1 to BBCH stage 6), indicating a great potential for sowing date monitoring during these periods.

5.2. Sowing Date Monitoring by Polarimetric Parameters in the Early Season

In this section, the sensitivity of different polarimetric parameters to the DAS was analyzed at different growing stages. As the analysis in the previous section shows, Stage A is not a suitable temporal window for sowing date monitoring, since SAR observations at this stage contain little vegetation information. The vegetative stages (BBCH stage 1 to stage 6) could be considered more useful for early season monitoring, whereas Stage D and Stage E seem too late, as the crop enters into the productive and ripening stages.

The relationship between the six parameters and the DAS was investigated using a subset of 66 randomly selected fields, by using the SAR acquisitions of 16 June or 10 July. Similar to the previous section, the 66 fields were divided into 17 groups according to their DAS and firstly each group of fields was averaged. The estimation model was constructed on the basis of the 17 average results. Then the sowing dates of the remaining 22 fields were predicted by the corresponding models. The results were validated by considering the actual sowing dates of the 22 fields and their RMSE values were obtained. The results of models obtained for the six scattering parameters at two different acquisition dated are presented in the Table 4.

On 16 June (Stage B), all the six parameters demonstrated significant sensitivity to the DAS (sowing dates), which could be satisfactorily fitted using linear models. The determination coefficient (R^2) of linear models for all the six parameters was very high (0.74–0.94), with a significance level of $P < 0.001$. The parameter Span (RMSE = 2.6 d) and Volume (RMSE = 2.4 d) provided better results than the last four parameters (Table 4). Especially, the Volume parameter showed the best estimation

accuracy. However, on July 10 (Stage C), the Volume parameter failed when constructing a linear model ($R^2 = 0.04$, $P > 0.05$). Although the Span parameter showed greater potential ($R^2 = 0.67$) at this stage, the estimation accuracy was not high (RMSE = 6.9 d). By contrast, the last four relative parameters (Volume/Total, Odd/Total, Entropy, and Alpha) demonstrated better results relying on linear models at this stage, with the RMSE from 2.8 to 3.9 d.

Table 4. Results of linear models for the prediction of sowing dates from the six scattering parameters at different SAR acquisition dates. In the linear models, the dependent variable (y) is DAS and the independent variable (x) is the scattering parameter value.

Acquisition Date	Parameters	66 Fields for Calibration		22 Fields for Validation
		Linear Model	R²	RMSE (d)
16 June	Span	y = 0.0152x − 0.2353	0.91	2.6
	Volume	y = 0.0106x − 0.2004	0.94	2.4
	Volume/Total	y = 0.0123x + 0.1155	0.76	5.8
	Odd/Total	y = −0.0109x + 0.8183	0.74	6.1
	Entropy	y = 0.0083x + 0.4122	0.81	5.8
	Alpha	y = 0.4311x + 14.652	0.78	6.8
10 July	Span	y = −0.0046x + 0.526	0.67	6.9
	Volume	y = −0.0006x + 0.2688	0.04	-
	Volume/Total	y = 0.0103x + 0.29	0.81	2.8
	Odd/Total	y = −0.0112x + 0.7167	0.84	2.9
	Entropy	y = 0.005x + 0.6117	0.77	3.9
	Alpha	y = 0.5499x + 15.143	0.84	3.3
16 June and 10 July	Volume/Total	y = 0.0144x + 0.0658	0.95	3.1
	Odd/Total	y = −0.0149x + 0.9196	0.95	3.1
	Entropy	y = 0.0087x + 0.4094	0.94	3.9
	Alpha	y = 0.674x + 8.1788	0.95	3.2

As the previous section showed (Figure 5), the last four parameters increased linearly and consecutively with the DAS during the vegetative stages (from BBCH stage 1–6). When the data of 16 June and 10 July were investigated together, it revealed, as expected, that the relationship between the polarimetric parameter and DAS during the entire vegetative stages can be well characterized just by a simple linear model, with high R^2 (significance $P < 0.001$). The estimation error was also low for the four parameters (Table 4), with the RMSE from 3.1 to 3.9 d. It meant that the linear model was feasible at any temporal window during the vegetative stages. The temporal window will be wide enough for more date choice of SAR acquisitions. It was essential for sowing date estimation in the practical application when the acquisition date of SAR image was limited to its revisit time.

5.3. Mapping Result of Oilseed Rape Fields

In this section, the estimation result of the sowing date of each oilseed rape field in Shangkuli farmland was mapped as a demonstration of the potential of this approach for spatial applications. Since the Volume parameter, at the 16 June acquisition date, revealed the highest estimation accuracy (Table 4), it was selected for sowing date mapping. The linear model was applied to estimate the sowing date of each oilseed rape field in this farmland. The estimation model is as follows:

$$y = T - (x + 0.2004)/0.0106 \qquad\qquad (2)$$

In the Equation, y is the sowing date of each field, x is the average volume scattering component of each oilseed rape field, and T is the current SAR observation date. Firstly, the average volume scattering of every oilseed rape field was inverted into DAS. Then the corresponding sowing date of each field was calculated according to DAS and the current observation time. With this, the sowing dates of all 88 oilseed rape fields in the farmland could be estimated based on SAR data acquired on June 16. For a better comparison, the estimation error (absolute error) of the sowing date was also calculated for each field. The ground truth data of the sowing dates of these 88 oilseed rape fields was mapped in Figure 7a, while their corresponding estimation error was mapped in Figure 7b. Of the fields 72.7% had an error smaller than two days. As shown in Figure 8, the estimation result showed a high level of agreement with the ground truth data, with a determination coefficient (R^2) of 0.87, root mean square error (RMSE) of 1.9 days, and maximum error of 4.7 days. These results confirmed the great capability of the Volume parameter in estimating the sowing dates of oilseed rape fields.

5.4. Discussion

In this study, the temporal behavior of the polarimetric response of oilseed rape fields during the entire growing season was investigated and the change trend of six different polarimetric parameters with DAS was observed. The observation results provided a solid basis for determining the suitable temporal window and polarimetric parameters for sowing date monitoring. While most studies have presented the temporal evolution based on one single field or just a few fields [18,19,42,43], this study provided a more comprehensive temporal evolution analysis based on 88 fields, covering a wider range of field conditions (Table 3). More importantly, it took advantage of a high observation frequency in terms of DAS, covering overall a period encompassing 81% of the whole growing cycle. Relying on the dense observations, a near-continuous evolution behavior was obtained and a clear trend was observed, which was essential for determining the suitable temporal window for sowing date monitoring. Most previous research on SAR for crop phenology monitoring, was based on limited discrete observations [38,41]. Although Kim *et al.* [44,45] obtained a near-continuous season-long monitoring, they used a ground-based scatterometer and they focused on rice or wheat crops. In addition, the temporal behavior of oilseed rape was investigated in some researches [27,29–31], but these were only limited to analysis of simple backscattering coefficients (or their ratio), rather than polarimetric signatures.

The results of this study revealed a high sensitivity of different polarimetric parameters to the DAS at different growing stages, and a simple empirical method of monitoring sowing dates was proposed. Although Volume and Span parameter showed the best accuracy on 16 June, their model was limited to a short period of observation, requiring that. the growing stages of all the fields should be within this temporal window. If the sowing period lasts longer (e.g., more than one month), or not all the fields are within this temporal window when the image is acquired, the results of this method will be affected. By contrast, four other parameters (Volume/Total, Odd/Total, Entropy and Alpha) encompass a wider temporal window for sowing date monitoring. It was found that a suitable linear model could be derived from data covering the entire vegetative stages (from BBCH stage 1–6). Despite its estimation accuracy not being as high as for Span and Volume parameters on 16 June, it has greater potential in practical applications.

Figure 7. Sowing dates of 88 oilseed rape fields and their estimation error: (**a**) the ground truth data; (**b**) the estimation error result. Background is SPOT-6 multi-spectral image acquired on 3 September 2013 (Color composite: Band 2 (red), Band 3 (blue), and Band 1 (green)).
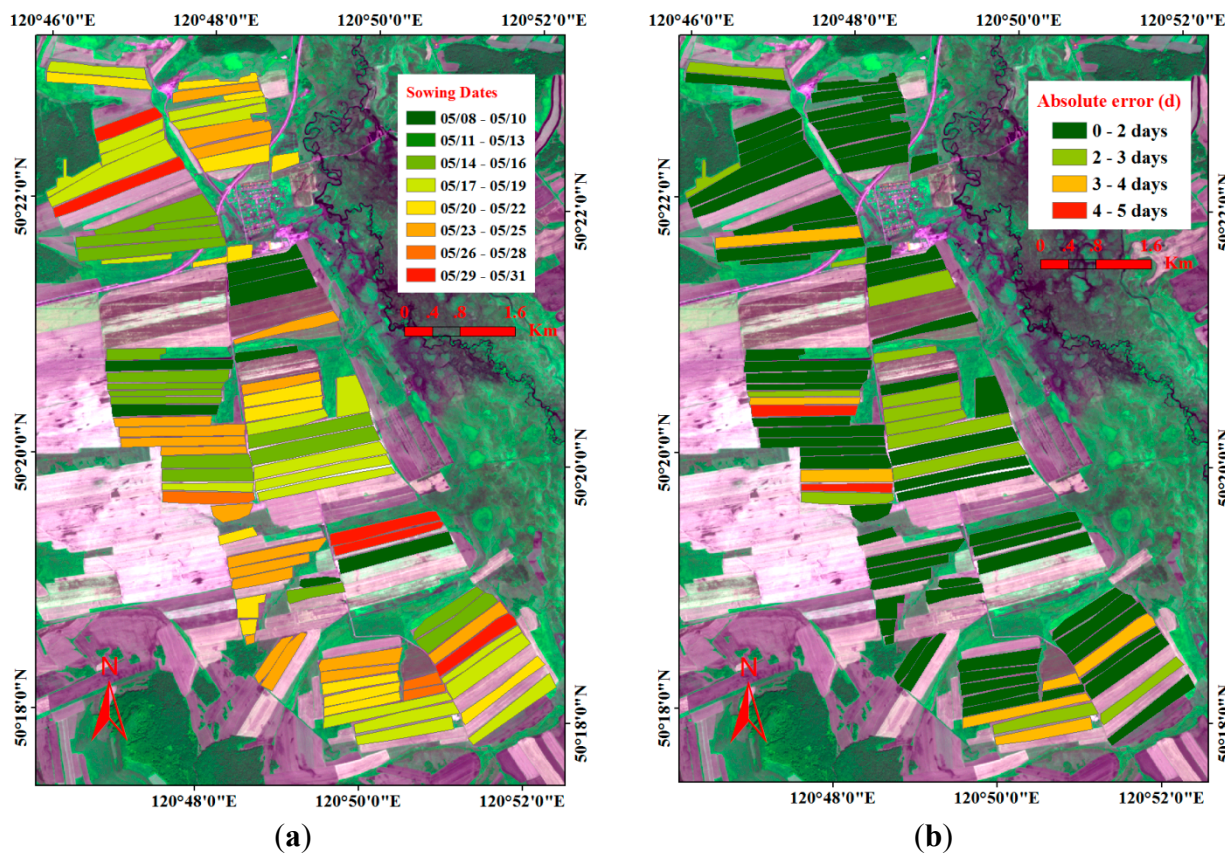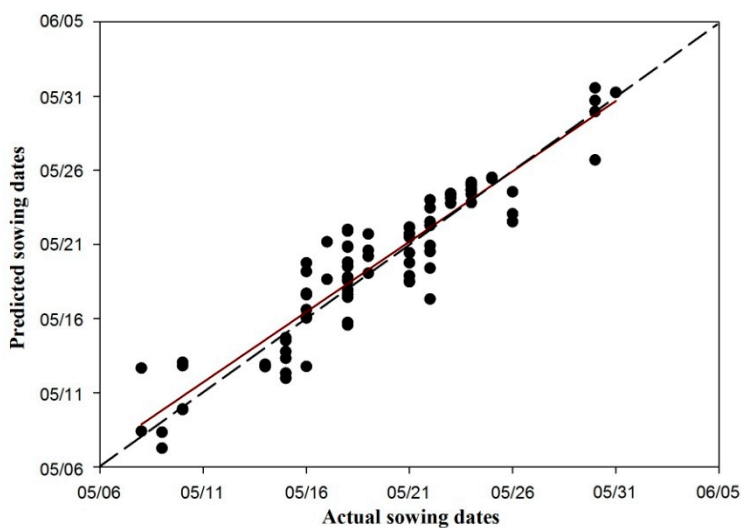

(**a**)   (**b**)

Figure 8. Comparison of ground truth *versus* estimation results. The dashed line (1:1 line) indicates the ideal estimation, and the solid line corresponds to the regression equation line. The circles indicate the corresponding fields.

Our sowing date estimation results were encouraging when compared to those reported by other studies, in terms of quality and consistency. For example Sakamoto *et al.* [13,46], despite the use of an elaborately designed algorithm for detecting rice, maize and soybean phenology, only obtained a

RMSE of 12.1 days (*n* = 30) for planting date. More recently, a RMSE of 3.2 days (*n* = 45) was obtained for wheat sowing date estimation in six states of India [47]. However, these results were obtained using geostationary satellite data, which are not available in most regions. In addition, Ortiz-Monasterio *et al.* [2] reported planting date estimates using Landsat data and a crop model in 100 wheat fields with RMSE = 6.5 days and R^2 = 0.85. Taking the complexity of the method into consideration, our method seems to be more promising for operational applications by end users. Nevertheless, since our model is empirical, it has to be calibrated with specific ground truth data, before it can be applied.

The potential capability of SAR data for monitoring crop growth and conditions was confirmed by this study, as has been reported that C-band SAR data is able to monitor dynamic processes of agricultural crops [29,48]. In this study, different sowing dates resulted in crop growth differences among different oilseed rape fields. SAR observation can effectively capture these growth differences. Therefore, the proposed method of monitoring sowing dates took advantage of the capability of SAR data in detecting crop growth. In contrast to optical sensors, SAR observations, especially their polarimetric features, can capture the growth differences through their effect on canopy structure, such as leaf area, plant height, vegetation biomass *etc.* Moreover, the SAR instrument is not constrained by rainy or cloudy weather, and it can provide more dependable data acquisitions for sowing date monitoring, especially considering current and also future SAR systems with short revisit time, e.g., Sentinel-1 (12 or 6 days) and ALOS-2 (14 days), TerraSAR-X (11 days).

6. Conclusions

The feasibility of using SAR data in early season to monitor sowing dates of oilseed rape crops was demonstrated in this paper. Five C-Band Radarsat-2 images in Fine Quad Mode were collected in the Shangkuli farmland area of China from 23 May to 27 August 2013, covering the entire growing cycle of oilseed rape. A set of polarimetric parameters was analyzed, including Volume, Span, Volume/Total, Odd/Total, Entropy and Alpha, relying on Freeman-Durden and Cloude-Pottier decomposition methods. Linear models could be used to estimate sowing dates at early growth stages (Table 4). This research has made a significant contribution to our understanding of polarimetric SAR response to oilseed rape crop development with time, illustrating the high sensitivity of polarimetric parameters to the DAS (day after sowing) at different growth stages. A near-continuous evolution behavior of six polarimetric parameters as a function of DAS during the entire growing season was obtained, based on ground data from 88 oilseed rape fields. The temporal trends of six polarimetric parameters during the whole growing season provided a solid basis for determining the most suitable temporal window and polarimetric parameters for sowing date monitoring.

Simple linear models can be used to monitor sowing dates at early growth stages, provided a suitable ground truth calibration is available. Volume and Span showed the best accuracy, with RMSE values of 2.4 days and 2.6 days respectively, at the stages of leaf development and formation of side shoots (BBCH stage 1 and BBCH stage 2), though their models were limited to a short temporal window. By contrast, it was found that four parameters (Volume/Total, Odd/Total, Entropy and Alpha) allowed the inclusion of a wider temporal window for sowing date monitoring. Their linear models were fairly accurate during the entire vegetative stages (from BBCH stage 1 to BBCH stage 6), with

RMSE smaller than four days. Moreover, they were less sensitive to changes in environmental conditions, which is critical when multiple images are available. Therefore, if we have prior information that all the oilseed rape fields are at the leaf development and formation of side shoots stages, Volume or Span parameter is suggested for sowing date monitoring. Otherwise, the four parameters will have greater potential in practical applications.

The results of this study highlight the importance of image acquisition date and polarization for crop monitoring based on SAR data. The result can not only help to identify the sowing dates in the region timely, but could also improve the regional estimation of crop yield and quality, as well as enable farmers to formulate the optimal strategies in farmland management to guarantee the yield.

Although this work has focused on the oilseed rape crop, the general approach may be applicable to other crops. Moreover, the results of this study were on a per-field basis, since a crop field map was available. However, the ambiguity produced by heterogeneity inside the field should be identified if the sowing date has to be estimated by pixel-wise approaches. From the point of view of the final application of this approach by the end users, it is necessary that a more complete validation in a different year or in a different region is carried out.

Further investigations are required to confirm these observations. In future studies, the application of this approach should be assessed over a more fragmented landscape and the adaptation of this method to other agricultural crops should be investigated.

Acknowledgments

Author Contributions

Hao Yang is the principal author of this manuscript having written the majority of the manuscript and contributed at all phases of the investigation. The other co-authors contributed in the field logistics, the field design, the selection and interpretation of the methods and contributed some portions of the written manuscript. The order of the authors reflects their level of contribution.

Conflicts of Interest

The authors declare no conflict of interest.

References

1. Ortiz-Monasterio, J.I.; Dhillon, S.S.; Fischer, R.A. Date of sowing effects on grain-yield and yield components of irrigated spring wheat cultivars and relationships with radiation and temperature in Ludhiana, India. *Field Crops Res.* **1994**, *37*, 169–184.

2. Ortiz-Monasterio, J.I.; Lobell, D.B. Remote sensing assessment of regional yield losses due to sub-optimal planting dates and fallow period weed management. *Field Crops Res.* **2007**, *101*, 80–87.

3. Lobell, D.B.; Ortiz-Monasterio, J.I.; Sibley, A.M.; Sohu, V.S. Satellite detection of earlier wheat sowing in India and implications for yield trends. *Agric. Syst.* **2013**, *115*, 137–143.

4. Muratova, N.; Terekhov, A. Estimation of spring crops sowing calendar dates using MODIS in Northern Kazakhstan. In Proceedings of 2004 IEEE International Geoscience and Remote Sensing Symposium, IGARSS '04, Anchorage, AK, USA, 20–24 September 2004; Volume 6, pp. 4019–4020.

5. Subedi, K.D.; Ma, B.L.; Xue, A.G. Planting date and nitrogen effects on grain yield and protein content of spring wheat. *Crop. Sci.* **2007**, *47*, 36–44.

6. Eslami, H.; Hadi, S.M.; Arabi, M.K. Effect of planting date on protein content of wheat varieties. *Int. J. Farming Allied Sci.* **2014**, *3*, 362–364.

7. Singh, S.; Gupta, A.K.; Gupta, S.K.; Kaur, N. Effect of sowing time on protein quality and starch pasting characteristics in wheat (*Triticum aestivum* L.) genotypes grown under irrigated and rain-fed conditions. *Food Chem.* **2010**, *122*, 559–565.

8. Leenhardt, D.; Lemaire, P. Estimating the spatial and temporal distribution of sowing dates for regional water management. *Agric. Water Manag.* **2002**, *55*, 37–52.

9. Moulin, S.; Bondeau, A.; Delecolle, R. Combining agricultural crop models and satellite observations: From field to regional scales. *Int. J. Remote Sens.* **1998**, *19*, 1021–1036.

10. Leinenkugel, P.; Kuenzer, C.; Oppelt, N.; Dech, S. Characterisation of land surface phenology and land cover based on moderate resolution satellite data in cloud prone areas—A novel product for the Mekong Basin. *Remote Sens. Environ.* **2013**, *136*, 180–198.

11. Tan, B.; Morisette, J.T.; Wolfe, R.E.; Gao, F.; Ederer, G.A.; Nightingale, J.; Pedelty, J.A. An enhanced TIMESAT algorithm for estimating vegetation phenology metrics from MODIS data. *IEEE. J. Sel. Top. Appl. Earth Obs.* **2011**, *4*, 361–371.

12. Wagenseil, H.; Samimi, C. Assessing spatio–temporal variations in plant phenology using Fourier analysis on NDVI time series: Results from a dry savannah environment in Namibia. *Int. J. Remote Sens.* **2006**, *27*, 3455–3471.

13. Sakamoto, T.; Yokozawa, M.; Toritani, H.; Shibayama, M.; Ishitsuka, N.; Ohno, H. A crop phenology detection method using time-series MODIS data. *Remote Sens. Environ.* **2005**, *96*, 366–374.

14. Wu, W.B.; Yang, P.; Tang, H.J.; Zhou, Q.B.; Chen, Z.X.; Shibasaki, R. Characterizing spatial patterns of phenology in cropland of China based on remotely sensed data. *Agric. Sci. China* **2010**, *9*, 101–112.

15. Mattia, F.; le Toan, T.; Picard, G.; Posa, F.I.; D'Alessio, A.; Notarnicola, C.; Pasquariello, G. Multitemporal C-band radar measurements on wheat fields. *IEEE Trans. Geosci. Remote Sens.* **2003**, *41*, 1551–1560.

16. Liu, C.; Shang, J.; Vachon P.W.; McNairn H. Multiyear crop monitoring using polarimetric Radarsat-2 data. *IEEE Trans. Geosci. Remote Sens.* **2013**, *51*, 2227–2240.

17. Shi, L.; Zhang, L.; Yang, J.; Zhang, L.; Li, P. Supervised graph embedding for polarimetric SAR image classification. *IEEE Geosci. Remote Sens. Lett.* **2013**, *10*, 216–220.

18. Lopez-Sanchez, J.M.; Cloude, S.R.; Ballester-Berman, J.D. Rice phenology monitoring by means of SAR polarimetry at X-band. *IEEE Trans. Geosci. Remote Sens.* **2012**, *50,* 2695–2709.

19. Lopez-Sanchez, J.M.; Vicente-Guijalba, F.; Ballester-Berman, J.D.; Cloude, S.R. Polarimetric response of rice fields at C-band: Analysis and phenology retrieval. *IEEE Trans. Geosci. Remote Sens.* **2014**, *52*, 2977–2993.

20. McNairn, H.; Hochheim, K.; Rabe, N. Applying polarimetric radar imagery for mapping the productivity of wheat crops. *Can. J. Remote Sens.* **2004**, *30*, 517–524.

21. Hajnsek, I.; Jagdhuber, T.; Schon, H.; Papathanassiou, K.P. Potential of estimating soil moisture under vegetation cover by means of PolSAR. *IEEE Trans. Geosci. Remote Sens.* **2009**, *47*, 442–454.

22. Cloude, S.R. *Polarisation: Applications in Remote Sensing*; Oxford University Press: Oxford, UK, 2009.

23. Adams, J.R.; Rowlandson, T.L.; McKeown, S.J.; Berg, A.A.; McNairn, H.; Sweeney, S.J. Evaluating the Cloude–Pottier and Freeman–Durden scattering decompositions for distinguishing between unharvested and post-harvest agricultural fields. *Can. J. Remote Sens.* **2013**, *39*, 318–327.

24. Cloude, S.R.; Pottier, E. An entropy based classification scheme for land applications of polarimetric SAR. *IEEE Trans. Geosci. Remote Sens.* **1997**, *35*, 68–78.

25. Freeman, A.; Durden, S.L. A three-component scattering model for polarimetric SAR data. *IEEE Trans. Geosci. Remote Sens.* **1998**, *36*, 963–973.

26. Vicente-Guijalba, F.; Martinez-Marin, T.; Lopez-Sanchez, J.M. Crop phenology estimation using a multitemporal model and a Kalman filtering strategy. *IEEE Geosci. Remote Sens. Lett.* **2014**, *11*, 1081–1085.

27. Fieuzal, R.; Baup, F.; Marais-Sicre, C. Monitoring wheat and rapeseed by using synchronous optical and radar satellite data—From temporal signatures to crop parameters estimation. *Adv. Remote Sens.* **2013**, *2*, 162–180.

28. Wiseman, G.; McNairn, H.; Homayouni, S.; Shang, J. RADARSAT-2 Polarimetric SAR response to crop biomass for agricultural production monitoring. *IEEE. J. Sel. Top. Appl. Earth Obs.* **2014**, doi:10.1109/JSTARS.2014.2322311.

29. Larranaga, A.; Alvarez-Mozos, J.; Albizua, L.; Peters, J. Backscattering behavior of rain-fed crops along the growing season. *IEEE Geosci. Remote Sens. Lett.* **2013**, *10*, 386–390.

30. Balenzano, A.; Mattia, F.; Satalino, G.; Davidson, M. Dense temporal series of C- and L-band SAR data for soil moisture retrieval over agricultural crops. *IEEE. J. Sel. Top. Appl. Earth Obs.* **2011**, *4*, 439–450.

31. Satalino, G.; Balenzano, A.; Mattia, F.; Davidson, M. C-band SAR data for mapping crops dominated by surface or volume scattering. *IEEE Geosci. Remote Sens. Lett.* **2013**, *11*, 384–388.

32. Meier, U. Growth Stages of Mono-and Dicotyledonous Plants. Available online: http://www.bba.de/veroeff/bbch/bbcheng.pdf (accessed on 17 October 2014).

33. Koppe, W.; Gnyp, M.L.; Hütt, C.; Yao, Y.; Miao, Y.; Chen, X.; Bareth, G. Rice monitoring with multi-temporal and dual-polarimetric TerraSAR-X data. *Int. J. Appl. Earth Obs. Geoinf.* **2013**, *21*, 568–576.

34. Lee, J.S.; Pottier, E. *Polarimetric Radar Imaging: From Basics to Applications*; CRC Press, Taylor & Francis Group: New York, NY, USA, 2009.

35. Sheng, Y.; Alsdorf, D.E. Automated georeferencing and orthorectification of Amazon basin-wide SAR mosaics using SRTM DEM data. *IEEE Trans. Geosci. Remote Sens.* **2005**, *43*, 1929–1940.

36. Gens, R.; Pottier, E.; Atwood, D.K. Geocoding of polarimetric processing results: Alternative processing strategies. *Remote Sens. Lett.* **2013**, *4*, 39–45.

37. Boerner, W.M.; Mott, H.; Livingstone, C.; Brisco, B.; Brown, R.; Paterson, J.S.; Luneburg, E.; van Zyl, J.J.; Randall, D.; Budkewitsch, P. Polarimetry in remote sensing: Basic and applied concepts. In *The Manual of Remote Sensing: Principles and Applications of Imaging Radar*, 3rd ed.; Ryerson, R.A., Ed.; American Society for Photogrammetry and Remote Sensing: Bethesda, MD, USA, 1998; pp. 271–357.

38. Cable, J.; Kovacs, J.; Jiao, X.; Shang, J. Agricultural monitoring in northeastern Ontario, Canada, using multi-temporal polarimetric RADARSAT-2 Data. *Remote Sens.* **2014**, *6*, 2343–2371.

39. Wang, X.; Ge, L.; Li, X. Pasture monitoring using SAR with COSMO-SkyMed, ENVISAT ASAR, and ALOS PALSAR in Otway, Australia. *Remote Sens.* **2013**, *5*, 3611–3636.

40. Ali, I.; Schuster, C.; Zebisch, M.; Forster, M.; Kleinschmit, B.; Notarnicola, C. First results of monitoring nature conservation sites in alpine region by using very high resolution (VHR) X-band SAR data. *IEEE. J. Sel. Top. Appl. Earth Obs.* **2013**, *6*, 2265–2274.

41. McNairn, H.; Wiseman, G.; Powers, J.; Merzouki, A.; Shang, J. Assessment of disease risk in oilseed rape using multi-frequency SAR: Preliminary results. In Proceedings of EUSAR 2014—10th European Conference on Synthetic Aperture Radar, Berlin, Germany, 2–6 June 2014; pp. 747–750.

42. Li, K.; Brisco, B.; Yun, S.; Touzi, R. Polarimetric decomposition with RADARSAT-2 for rice mapping and monitoring. *Can. J. Remote Sens.* **2012**, *38*, 169–179.

43. Lopez-Sanchez, J.M.; Ballester-Berman, J.D.; Hajnsek, I. First results of rice monitoring practices in Spain by means of time series of TerraSAR-X dual-pol images. *IEEE. J. Sel. Top. Appl. Earth Obs.* **2011**, *4*, 412–422.

44. Kim, Y.; Lee, H.; Hong, S. Continuous monitoring of rice growth with a stable ground-based scatterometer system. *IEEE Geosci. Remote Sens. Lett.* **2013**, *10*, 831–835.

45. Kim, Y.; Jackson, T.; Bindlish, R.; Hong, S.; Jung, G.; Lee, K. Retrieval of wheat growth parameters with radar vegetation indices. *IEEE Geosci. Remote Sens. Lett.* **2014**, *11*, 808–812.

46. Sakamoto, T.; Wardlow, B.D.; Gitelson, A.A.; Verma, S.B.; Suyker, A.E.; Arkebauer, T.J. A two-step filtering approach for detecting maize and soybean phenology with time-series MODIS data. *Remote Sens. Environ.* **2010**, *114*, 2146–2159.

47. Vyas, S.; Nigam, R.; Patel, N.K.; Panigrahy, S. Extracting regional pattern of wheat sowing dates using multispectral and high temporal observations from Indian geostationary satellite. *J. Indian Soc. Remote Sens.* **2013**, *41*, 855–864.

48. Inoue, Y.; Sakaiya, E.; Wang, C. Capability of C-band backscattering coefficients from high-resolution satellite SAR sensors to assess biophysical variables in paddy rice. *Remote Sens. Environ.* **2014**, *140*, 257–266.